ELSEVIER

Journal of Molecular Catalysis A: Chemical 135 (1998) 295–306

JOURNAL OF MOLECULAR CATALYSIS A: CHEMICAL

Zeolite-encapsulated manganese(III)salen complexes

Saji P. Varkey, Chandra Ratnasamy, Paul Ratnasamy *

National Chemical Laboratory, Pune 411008, India

Received 16 June 1997; accepted 5 December 1997

Abstract

Manganese(III) complexes of [*N*,*N*′-ethylenebis(salicylidene-aminato)] (salen), [*N*,*N*′-ethylenebis(5-chloro-salicylidene-aminato)] (Cl_2Salen), [*N*,*N*′-ethylenebis(5-bromo-salicylidene-aminato)] (Br_2Salen) and [*N*,*N*′-ethylenebis(5-nitro-salicylidene-aminato)] [$(NO_2)_2$Salen] have been encapsulated in the supercages of zeolite X by the zeolite synthesis method. The catalysts have been characterized by FTIR, UV–Vis and EPR spectroscopic techniques, XRD, SEM, thermal and elemental analysis, as well as nitrogen adsorption and cyclic voltammetric studies. The extent of encapsulation of the Mn(III)Salen complexes in zeolite X varies with the nature of the substituent group on the aromatic ring. While bromo groups enhance encapsulation, substitution with $-NO_2$ groups decreases the amounts of Mn(III) complexes encapsulated in the cavities of the zeolites. Cyclic voltammetric data indicate that the zeolite matrix facilitates the reduction of Mn(III) to Mn(II), suggesting that it behaves like an electron-withdrawing substituent. The aerobic oxidation of styrene to benzaldehyde, styrene oxide and phenylacetaldehyde over these catalysts is also reported.

Keywords: Mn(III)Salen; Zeozymes; Ship-in-a-bottle complexes; Oxidation catalysts; *N*,*N*′-Ethylenebis(salicylidene amines); Styrene oxidation

1. Introduction

Zeolite-encapsulated, transition metal complexes are currently under study as functional mimics of enzymes [1–5], heterogeneous catalysts [6,7] and as electrocatalysts [8]. The encapsulation of manganese salen complexes in Na–Y zeolite by the flexible ligand method (synthesis of the metal complex in situ in the zeolite cavity by reaction of the ligand with the exchanged metal cations) has already been reported [7]. Metal complexes have also been encapsulated by the synthesis of the zeolite in the presence of the preformed metal complexes (the so called 'zeolite synthesis' method) [8]. The zeolite synthesis method has been employed to encapsulate metal complexes in a variety of molecular sieves ranging from the small pore clathrasil to the large pore faujasite-type zeolites. The latter are well-suited for the preparation of encapsulated complexes because of the large supercage (diameter ~ 12 Å) and the restricted pore opening (~ 7.4 Å) to this supercage.

The catalytic activity especially in selective, low-temperature oxidation reactions, of homo-

* Corresponding author. Fax: +91-212-330233; e-mail: prs@ems.ncl.res.in

1381-1169/98/$ - see front matter
PII: S1381-1169(97)00307-5

geneous manganese salen complexes, has been extensively investigated [9–11]. Substituted Jacobsen-type, manganese salen catalysts for the regio- and enantioselective oxidation of olefins [12,13] are emerging as major catalyst systems in the pharmaceutical industry. What are the catalytic consequences of encapsulating such catalysts in shape-selective, zeolite materials? Can we modify the spatio-, regio-, or enantioselective features of these complexes by a proper choice of the microporous structure of the zeolite? Since electron-withdrawing substituents on the salen ligands affect their encapsulation and catalytic activity, we would like to know if the consequent depleted electron density at the metal centre and the distorted geometry of the complex (the latter arising out of the geometric constraints inside the zeolite cavities) are associated with unusual structural and/or catalytic properties in oxidation reactions.

The present paper describes the synthesis and physicochemical characterization and catalytic activity in the aerobic oxidation of styrene of various salen complexes containing, on the 3- and/or 5-positions, electron-withdrawing groups like –Cl, –Br or $–NO_2$ and encapsulated in zeolite X by the 'zeolite synthesis' method.

2. Experimental

2.1. Materials and methods

Fumed silica, sodium hydroxide, lithium chloride, potassium chloride, salicylaldehyde, 5-bromosalicylaldehyde, 5-chlorosalicylaldehyde, 5-nitrosalicylaldehyde, were purchased from Aldrich Chem. and used as such. Aluminium isopropoxide (Fluka), manganese acetate tetrahydrate (E. Merck), tetrabutyl ammonium tetrafluoroborate (Sigma) were commercially available pure samples and used without further purification. All the solvents (dimethyl sulphoxide, acetonitrile, ethyl alcohol) were distilled before use.

2.2. Catalyst preparation

2.2.1. General procedure for the preparation of ligands

The salicylaldehyde derivative 1 (Fig. 1) (2.0 equivalent) was added to a 0.2-M solution of ethylene diamine (1.0 equivalent) in absolute alcohol. The mixture was heated to reflux for 1 h and the bright yellow crystalline solid (salen or substituted salen) formed was collected by

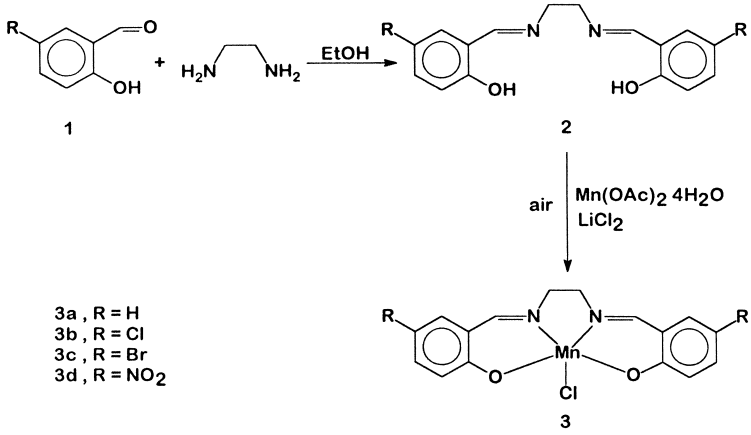

Fig. 1. Preparation of manganese salens.

filtration and washed with a small portion of 95% ethanol. The yields of analytically pure salen ligand (Fig. 1) obtained in this manner were in the range of 90–95%. Acceptable C, H, N analyses have been obtained.

2.2.2. General procedure for the preparation of neat metal complex catalysts (Fig. 1)

The ligand 2 obtained in the above manner was redissolved in hot absolute ethanol to give a 0.1-M solution. Solid hydrated manganese(II) acetate (2.0 equivalent) was added in one portion and the solution was refluxed for 1 h. Approximately three equivalents of lithium chloride was then added, and the mixture is heated to reflux for an additional 0.5 h. Cooling the mixture to 273 K affords the Mn(III) complexes (3a–3d) as dark brown crystals. They were washed thoroughly with water and isolated by filtration in $\sim$ 75% yield. An additional crop of materials can be isolated by dropwise addition of water to the mother liquor. Yields of catalysts 3a–3d were in the range 82–91%. Satisfactory elemental analyses were obtained for these metal complexes.

2.2.3. General procedure for the encapsulation of metal complexes in Na–X type zeolite by the zeolite synthesis method

Before we discuss the synthetic procedure for encapsulation, the solubility of metal complexes in the synthesis medium should be established. Only dissolved manganese salen complexes in solution can be encapsulated in microporous cavities during zeolite synthesis. We have measured the solubility of Mn(III)Salen complex in the zeolite synthesis medium to confirm the feasibility of encapsulation of complexes in zeolite cages by the zeolite synthesis method. Mn(III)Salen (0.3 g; containing 4.6×10^{-2} g of Mn) was stirred in 100 g of an aqueous solution of fumed silica and NaOH (pH = 12.8) at room temperature for 24 h, before heating at 363 K for 24 h. This solution was identical to that used during the synthesis of zeolite X, except that the Al source was not added. The latter precaution was taken in order to avoid the precipitation of an aluminosilicate solid. At the end of 12 h, 0.15 g of the solid Mn(III)Salen (equivalent to 0.0335 g of Mn was recovered by centrifugation (8000 rpm for 2 h) of the hot slurry. Chemical analysis of the clear, solution (by atomic absorption spectroscopy) revealed the presence of 0.0335 g of Mn in 100 g of the clear solution. In most of the encapsulation experiments, the yield of solid zeolite from 100 g such a solution was 5–10 wt.%. Since the manganese content in MnSal–X was 0.33 wt.% (Table 1) (equivalent to about 0.0033 g of Mn), it may be concluded that the zeolite synthesis medium contained enough dissolved MnSalen complex to lead to the encapsulation levels observed for MnSal–X. Similar results were obtained for other complexes.

The general procedure for the encapsulation of metal complexes is next described. The silicate gel was prepared from 4.0 g of fumed silica, 3.2 g of NaOH, 0.30 g of the appropriate manganese salen complexes and 8.0 ml of H_2O and stirred for 30 min. To the above solution, sodium aluminate (prepared from 9 g of Al (iOPr)3, 3.2 g of NaOH and 36 ml of H_2O) was added. The resulting gel was then transferred to a polypropylene bottle and aged at room temperature with stirring for 24 h and then heated at 363 K for 24 h. The mixture was then allowed to cool to room temperature and diluted with copious amounts of deionized water. The solid crystals were isolated by centrifugation at 8000 rpm for 2 h. This solid was dried at 363 K for 24 h in air and extracted (Soxhlet) with acetonitrile for 72 h. It was finally dried at 363 K

Table 1
Metal content (wt.%) of zeolite-encapsulated Mn(III)LCl–X catalysts[a]

Catalyst L	Si	Al	Na	Mn
Salen	24.7	19.4	10.4	0.33
Cl_2Salen	23.4	14.2	14.9	0.26
Br_2Salen	26.6	11.2	06.4	0.37
$(NO_2)_2$Salen	24.5	12.2	09.0	0.24

[a] Mn(III)LCl encapsulated in zeolite X.

under vacuum (1×10^{-3} Torr) for 15 h. The catalysts are designated by: Metal (formal oxidation state) Ligand–Zeolite. Thus, Mn(III) Cl_2Salen–X designates a 5,5′-dichlorosalen complex of Mn(III) with an axial chlorine ligand encapsulated in zeolite X.

2.3. Catalyst characterization

The FTIR spectra of the solid catalysts and the neat complexes were recorded in nujol mulls using a Perkin-Elmer 1600 FTIR spectrophotometer. The diffuse reflectance spectra were recorded with a Shimadzu UV-2101 PC UV–Vis spectrophotometer using $BaSO_4$ as an internal standard. Simultaneous TG–DTA–DTG analyses of the neat metal complexes as well as the zeolite-encapsulated metal complexes were recorded on an automatic derivatograph, Setaram TG–DTA 92. Scanning electron micrographs of the solid catalysts were recorded using a Leica Stereoscan-440, Cambridge Instrument. The X-ray powder patterns of the samples were obtained with a Rigaku Model D/MAX III VC, Japan. Data were collected in the 2θ range 4–48° at a scan rate of 8°/min. Silicon was used as the internal standard for calibrating the instrument. The X band ESR spectra of the solid catalysts were measured at room temperature and liquid nitrogen temperature using a Bruker E-2000 ESR spectrometer (200D). Chemical analysis for Mn, Si, Al and Na were done by atomic absorption spectrometer (Hitachi Model Z-8000). The C, H, N analyses (of the metal complexes) were obtained from Carlo ERBA (Italy) Model EA 1108 analyser. Omnisorb 100 CX (Coulter, USA) was used for the N_2 adsorption measurements. The samples were activated at 373 K for 4 h, in high vacuum (1.33×10^{-6} Pa) prior to adsorption measurements. All electrochemical studies were performed at 25°C with a three-electrode potentiostatic system (EG and G Model 362). The working electrode was a graphite paste electrode containing the neat and zeolite-encapsulated complexes. The potentials are expressed with reference to an aqueous saturated calomel electrode placed in a separate compartment containing the supporting electrolyte. Electrolytic solutions DMSO/Bu_4NBF_4($TBABF_4$) and H_2O/KCl (both 1 mmol) were routinely deoxygenated with argon. The modified graphite paste electrode containing the neat and zeolite encapsulated metal complexes were prepared by adding 20 mg of the respective catalyst to 20 mg of the graphite powder. The mixture was then mixed thoroughly and applied as a paste on a platinum wire.

2.4. Catalytic activity

Oxidation reactions were carried out in a thermostated reactor of 100 ml volume. The reactor was equipped with a reflux condenser and a gas inlet. In a typical experiment, dry air was bubbled through the reactor under normal pressure, and 0.1 g of the desired catalyst was introduced. Five grams of acetonitrile, 5 g of styrene and 0.1 g of tertiary butyl hydroperoxide was added, and the reaction was carried out in a 100 ml reactor for 10–12 h at 343 K. At the end of the reaction, the reaction mixture was cooled to room temperature, and the products were analysed in a gas chromatograph (Shimadzu GC 14B) equipped with a SE-52 column. The identity of the products was further confirmed by GCMS (Shimadzu GCMS QP 5400).

3. Results and discussion

3.1. Chemical analysis

The metal contents of the catalysts are given in Table 1. The Si/Al ratios are in the range of those expected for faujasites. In addition to traditional chemical analysis, the amount of salen or substituted salen ligands from the encapsulated Mn(III) complexes were estimated quantitatively by UV–Vis spectroscopy after digestion of 0.1 g of the zeolite containing the

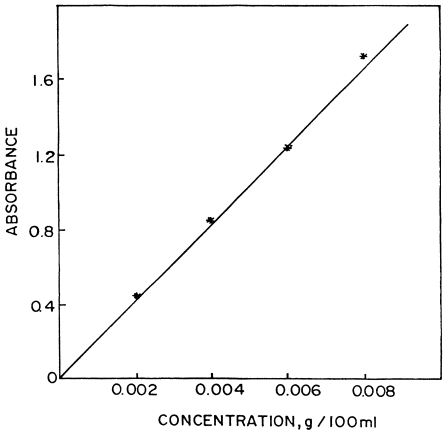

Fig. 2. Calibration curve for estimating salen in zeolite by UV–Vis diffuse reflectance spectroscopy.

encapsulated complex in 100 ml Con · H_2SO_4 (for 2 h). The concentration of Mn(III)Salen was calculated from a calibration curve. Fig. 2 shows a typical calibration curve for Mn(III)Salen–X. Such calibration curves were drawn for each of the salen complexes studied. The salen concentration of encapsulated complexes estimated from such calibration graphs were in agreement with the Mn content estimated by atomic absorption spectrometry, indicating that the stoichiometric integrity of the complex had been maintained during the zeolite synthesis process.

3.2. X-ray diffraction and scanning electron microscopy

The X-ray diffractograms of the catalysts containing the Mn(III) complexes (Fig. 3) did not reveal any significant difference from those of NaX. The encapsulation of the manganese complexes inside the zeolite cavities is indicated by the absence of extraneous material by scanning electron microscopy (SEM). Both X-ray diffraction and SEM indicate that zeolites with good crystallinity can be obtained during the encapsulation of MnSalen complexes by the zeolite synthesis method. From SEM, the average size of the zeolite particles was estimated to be about 1 μm.

3.3. IR spectroscopy

IR spectroscopy can also provide information on the integrity of the encapsulated complexes, as well as the crystallinity of the host zeolite. The IR bands of all encapsulated complexes are weak due to their low concentration in the

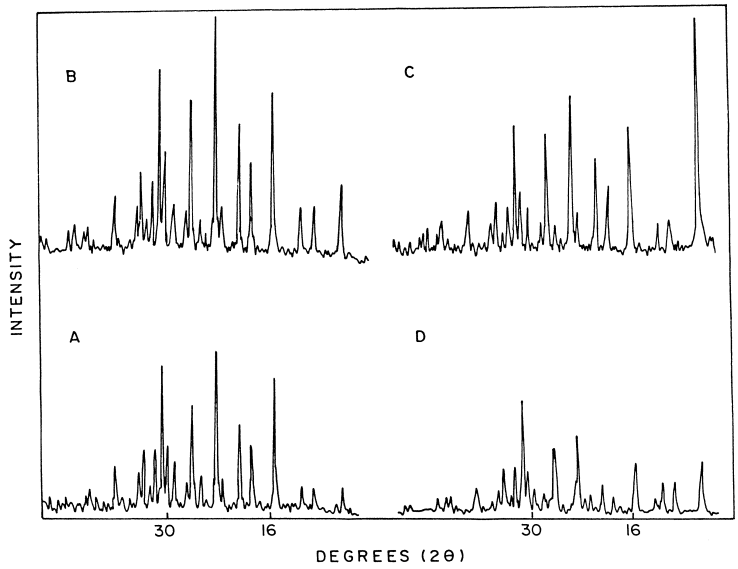

Fig. 3. Powder XRD patterns: (A) Mn(III)Salen–X; (B) Mn(III)Cl_2Salen–X; (C) Mn(III)Br_2Salen–X; (D) Mn(III)$(NO_2)_2$Salen–X.

Table 2
FTIR spectra (cm^{-1}) of the neat and encapsulated complexes[a]

Catalyst	$\nu_{C=C}$	ν_{C-H}	$\nu_{C=N}$	ν_{C-N}	ν_{C-O}	Ring vibration
Mn(III)Salen	1637 (s)	2926 (vs), 2856 (vs)	1555 (s)	1160 (s)	1060 (s)	1410 (s), 1080 (w), 730 (s)
Mn(III)Salen–X	1635 (m)	2930 (vs), 2880 (s)	1553 (m)	1165 (m)	1057 (s)	1412 (s), 1090 (w), 732 (w)
Mn(III)Cl_2Salen	1633 (s)	2940 (vs), 2895 (s)	1558 (s)	1167 (s)	1046 (s)	1414 (s), 1070 (s), 740 (s)
Mn(III)Cl_2Salen–X	1632 (m)	2950 (s), 2892 (m)	1558 (m)	1169 (m)	1050 (w)	1415 (s), 1072 (w), 737 (w)
Mn(III)Br_2Salen	1635 (s)	2932 (s), 2904 (s)	1561 (s)	1163 (m)	1054 (w)	1420 (s), 1076 (m), 740 (s)
Mn(III)Br_2Salen–X	1631 (m)	2935 (s), 2910 (m)	1557 (m)	1163 (m)	1056 (w)	1424 (s), 1076 (sh), 741 (w)
Mn(III)$(NO_2)_2$Salen	1637 (s)	2920 (vs), |2896 (vs)	1552 |(s)	1154 (s)	1056 (m)	1418 (s), 1073 (sh), 742 (w)
Mn(III)$(NO_2)_2$Salen–X	1636 (m)	|2923 (s) |2896 (s)	|1554|(m)	1156 (m)	1059 (s)	1419 (s), 1077 (sh), 746 (w)

w = weak; s = strong; vs = very strong; m = medium; sh = shoulder.

zeolite. Unlike phthalocyanine complexes, Mn(III)Salen complexes encapsulated in the zeolite cages did not show any significant shift in C=N or C=C stretching modes. The IR spectra show major bands around 1600, 1560, 1510, 1460, 1410, 1330, 1280, 1210, 1150 and 1090 cm^{-1}. We did not notice any appreciable changes in the frequencies of Mn(III)Salen complexes after incorporation into the zeolite matrix. The major FTIR bands of the catalysts are tabulated in Table 2.

3.4. EPR spectroscopy

The EPR spectra of neat and encapsulated Mn(III)Salen complexes at room temperature gave a single broad signal exhibiting $g_\perp$ and $g_\parallel$ values in the region 2.03–2.04 and 2.07–2.11, respectively. The g values of the encapsulated complexes were not shifted significantly from that of the neat complexes.

3.5. Diffuse reflectance spectra

The diffuse reflectance spectra of Mn(III) complexes of salen or substituted salens (Table 3) are almost identical before and after encapsulation, indicating that the complexes maintain their geometry even after encapsulation without significant distortion. The broad intense band observed around 515 nm region can be assigned to a d–d band arising from the $^5Eg \rightarrow {}^5T_2 g$ transition. The data are in good agreement with those reported [7] for similar Mn(III) systems.

3.6. Surface area / pore volume

The surface area and pore volume of the catalysts are shown in Table 4. The inclusion of Mn(III)Salen complexes dramatically reduces the adsorption capacity and the surface area of the zeolite. It has been reported [14] that the BET surface area of X and Y zeolite containing

Table 3
Diffuse reflectance spectra of the neat and the encapsulated complexes

Catalyst	Diffuse reflectance spectral data λ_{max} (nm)
Mn(III)Salen	508, 455, 410, 356, 311, 285, 248, 236
Mn(III)Salen–X	510, 402, 383, 355, 312, 287
Mn(III)Cl_2Salen	514, 448, 397, 352, 314, 285, 244, 212
Mn(III)Cl_2Salen–X	508, 421, 396, 359, 341, 306, 276
Mn(III)Br_2Salen	515, 455, 410, 359, 327, 311, 285, 248
Mn(III)Br_2Salen–X	520, 429, 374, 351, 324, 318, 282, 245
Mn(III)$(NO_2)_2$Salen	524, 427, 418, 391, 375, 348, 322, 308, 251
Mn(III)$(NO_2)_2$Salen–X	516, 420, 378, 339, 318, 296, 250

Table 4
Surface area and pore volume of catalysts

Catalyst	Surface area (m^2/g)	Pore volume (ml/g)
Mn(III)Salen–X	75	
Mn(III)Cl_2Salen–X	35	
Mn(III)Br_2Salen–X	135	0.0211
Mn(III)$(NO_2)_2$Salen–X	71	0.0165

phthalocyanine complexes are typically less than 100 $m^2\ g^{-1}$. The lowering of the pore volume and surface area indicate the presence of Mn(III)Salen complexes within the cavities of the zeolites and not on the external surface.

3.7. Thermal analysis

Differential thermal analysis and thermogravimetric analysis have been used to characterize intrazeolite metal complexes [15]. TG and DTA obtained for all the neat and the encapsulated complexes are depicted in Fig. 4. The neat complex Mn(III)Br_2Salen, for example, shows a weight loss at 320°C. However, for the corresponding encapsulated complex, there is a continuous weight loss that extends above 500°C. Similar behaviour was observed with Mn(III)Salen–X, Mn(III)Cl_2Salen–X and Mn(III)$(NO_2)_2$Salen–X samples also. The

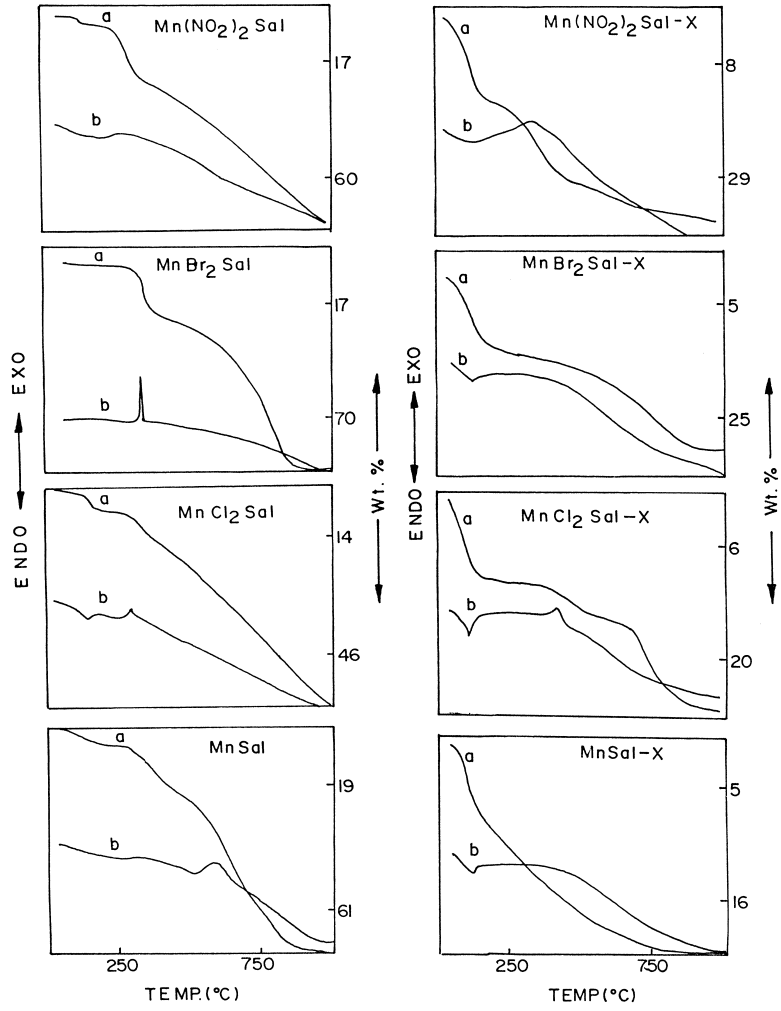

Fig. 4. Thermogravity (a) and differential thermal analysis (b) of samples.

thermal stability of the neat and the corresponding encapsulated complexes increase in the order Mn(III)Cl_2Salen > Mn(III)$(NO_2)_2$Salen > Mn(III)Salen > Mn(III)Br_2Salen and Mn(III)Salen–X > Mn(III)Cl_2Salen–X > Mn(III)Br_2Salen–X > Mn(III)$(NO_2)_2$Salen–X.

3.8. Electrochemical studies

Fig. 5 shows a comparison of the cyclic voltammograms for Mn(III)Br_2Salen complex in DMSO using 0.1 M $TBATBF_4$ as the supporting electrolyte (data in Table 5). Curve 1a indicates the voltammogram for the complex dissolved in the electrolyte using platinum working electrode at a scan rate of 20 mV/s. For comparison, curve 1b indicates the voltammogram using the zeolite pasted electrode containing the encapsulated Mn(III)Br_2Salen complex under identical conditions of scan rate (20 mV/s). The quasi-reversible signal observed for Mn(III) → Mn(II) at an $E_{1/2}$ value of −0.60 V for the pure complex is in agreement with the known electrochemical behaviour of the compounds [16]. This is further supported by the unequal magnitude of peak current and also by the shift of both the cathodic and anodic peak potentials with scan rate, (e.g., when the scan rate changes from 20 to 200 mV/s, the cathodic peak potential E_{pc} shifts from −0.94 to −1.22 V while the anodic peak potential E_{pa} shifts from −0.26 to −0.70 V). Further, the peak current after base line correction, when plotted against the square root of scan rate gives a straight line, indicating that the electrochemical behaviour is diffusion-controlled.

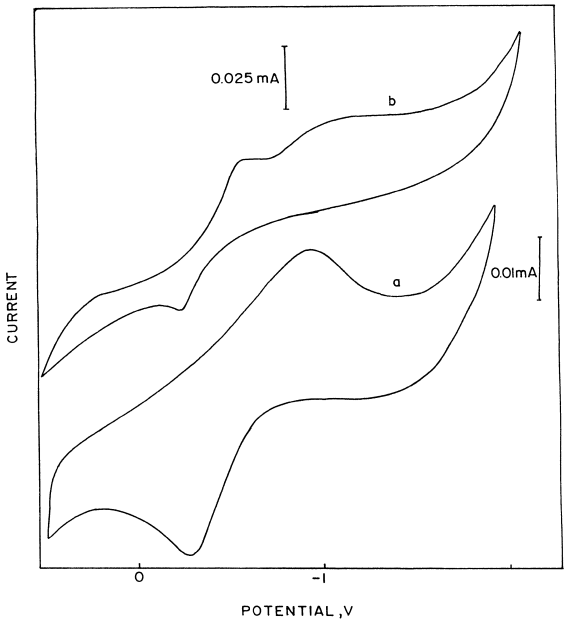

Fig. 5. Cyclic voltammogram of (a) Mn(III)Br_2Salen dissolved in 0.1 M DMSO/$TBABF_4$ and (b) graphite–Mn(III)Br_2Salen–X paste coated on platinum wire as electrode in 0.1 M DMSO/$TBATBF_4$ (scan rate $\Delta = \Delta 20$ mV/s).

Table 5
Electrochemical data for the neat (3c) and encapsulated (C) Mn(III)Br_2Salen complex in 0.1 M $TBATF_4$/DMSO system

Catalyst	Scan rate (mV/s)	$E_{1/2}$ (V)	E_{pc} (V)	E_{pa} (V)	ΔE_p (V)
3c[a]	20	−0.60	−0.94	−0.26	−0.68
C[b]	20	−0.42	−0.58	−0.26	−0.32
3c[a]	200	−0.96	−1.22	−0.70	−0.52
C[b]	200	−1.12	−1.26	−0.98	−0.28

[a]The neat complex dissolved in $TBATBF_4$/DMSO, working electrode is Pt wire.
[b]The zeolite-encapsulated complex mixed with graphite powder and coated on the Pt wire.

A closer examination of the CV behaviour in Fig. 5 indicates several interesting features as a result of the encapsulation of the metal complex in a zeolite matrix. For example, the $E_{1/2}$ value corresponding to Mn(III) → Mn(II) process is shifted from −0.60 to −0.42, indicating quantitatively the change in the relative stability of a 1:1 equilibrium mixture of both Mn(II) and Mn(III) complexes in the zeolite matrix. The potential separation between the cathodic and anodic peak is also considerably reduced (−0.68 to −0.32 V) when the complex is encapsulated in the zeolite matrix. In addition, as a result of encapsulation the E_{pc} values shift from −0.94 to −0.58 while E_{pa} values do not shift significantly (from −0.26). The zeolite matrix, thus, facilitates the reduction of Mn(III), suggesting that the matrix is, perhaps, behaving like an electron-withdrawing substituent. An additional small peak is also observed around −1.0 V

probably due to the presence of adsorbed species. A similar behaviour for other intrazeolite complexes is known [17]. When the scan rate is changed from 20 to 200 mV/s, the $E_{1/2}$ value for the neat complex shifts from -0.60 to -1.01 V ($\Delta = 300$ mV). The corresponding value for the encapsulated complex is 700 mV, indicating that the complex encapsulated in the zeolite is more sensitive to the external parameters such as time scale of potential variations.

Since several Mn porphyrin complexes [18,19] are soluble in water, and several Mn complexes exhibit multiple oxidation states in aqueous media, voltammograms were also taken in aqueous solution for comparison (Table 6). Fig. 6 shows the cyclic voltammogram of a graphite paste containing Mn(III)Br_2Salen complex in H_2O/KCl (a) and also the same complex encapsulated in zeolite X (b) at a scan rate of 10 mV/s using a method developed recently for insoluble compounds by Bond and Scholz [20]. The free complex exhibits a well defined pair of reversible peaks around $E_{1/2} = +0.04$ along with two irreversible oxidation peaks around -0.20 and -0.48 V, respectively. On encapsulation, the single reversible peak becomes sharper ($E_{1/2} = +0.05$) in comparison to that of the neat complex (Fig. 6). As a result of immobilization, the E_{pc} values of the complex shifts to less negative values (-0.06) while the corresponding E_{pa} value does not show a significant shift. This potential shift suggests that Mn(III) is more affected (60 mV) as a result of encapsulation compared to Mn(IV)

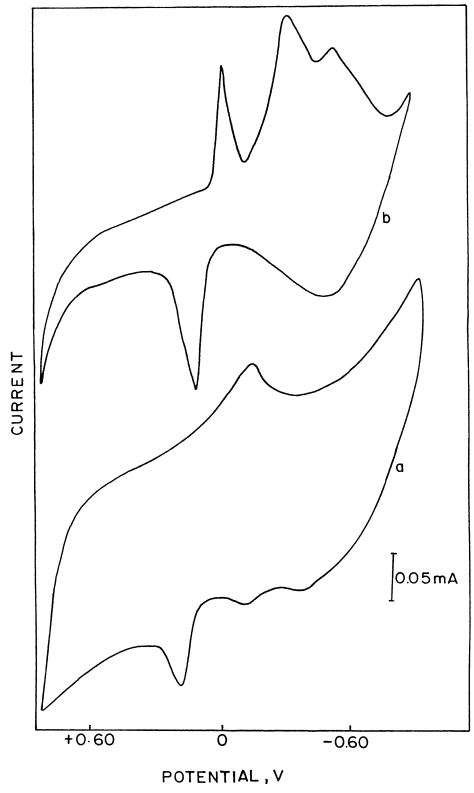

Fig. 6. Cyclic voltammogram of (a) graphite–Mn(III)Br_2Salen electrode and (b) graphite–Mn(III)Br_2Salen–X electrode in 0.1 M KCl/H_2O (scan rate $\Delta = \Delta 10$ mV/s).

Table 6
Electrochemical data for the neat (3c) and the encapsulated (C) Mn(III)Br_2Salen complex in H_2O/KCl system

Catalyst	Scan rate (mV/s)	$E_{1/2}$ (V)	E_{pc} (V)	E_{pa} (V)	ΔE_p (V)
3c	10	+0.04	−0.10	+0.17	+0.07
C	10	+0.05	−0.06	+0.16	+0.10
3c	200	+0.04	−0.22	+0.30	+0.08
C	200	−0.28	−0.42	+0.26	−0.16

[a]Working electrode: neat or the encapsulated complex mixed with graphite powder and pasted on Pt wire.

presumably due to the change in coordinating behaviour. Additionally, another two broad irreversible reduction peaks at -0.40 and -0.60 V are observed, which are absent for the free complex. This may be due to the accessibility of other reduction states such as Mn(II) in aqueous medium. More interestingly, the cathodic peak around -0.48 show features such as broadening and asymmetry in shape typical for adsorption peaks [21].

3.9. Catalytic activity

Experimental evidence that the oxidation of styrene is catalysed predominantly by the solid zeolite containing the encapsulated $MnBr_2$ salen complex is presented in Fig. 7. In one of a set of two identical experiments, the solid catalyst was

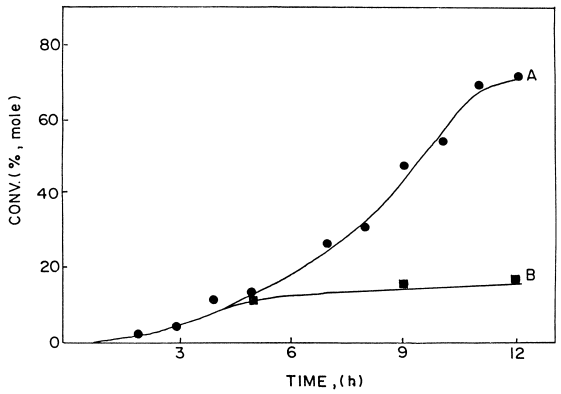

Fig. 7. Kinetics of styrene oxidation in the presence of solid catalyst $MnBr_2$Salen–X (A) and when the catalyst is removed from the reaction mixture at 4 h reaction time (B).

removed by filtration at a reaction time of 4 h. While the oxidation of styrene continued in the presence of the catalyst (Fig. 7A), there was no further significant conversion when the catalyst was removed from the reaction system (Fig. 4B). This conclusion was independently confirmed by the absence of manganese in the filtrate (atomic absorption spectroscopy). In general, it was observed that the extent of leaching of the salen complex in the reaction mixture depended, among other things, on the number and nature (especially size) of the substituents on the salen ligand.

The results of the oxidation of styrene using O_2 as the oxidant, *tert*-butyl-hydroperoxide (TBHP) as the initiator (2 wt.% of styrene) and acetonitrile as the solvent at 343 K over the various manganese salens, both in the neat and in the encapsulated state, are presented in Table 7. The following points may be noted. (1) The major products of oxidation of styrene are benzaldehyde, styrene oxide and phenyl acetaldehyde with minor amounts of benzoic acid and benzene-1,2-ethane diol. In some experiments, especially at high temperatures, polymer formation was also observed. (2) The zeolite-encapsulated complex did not undergo any colour change during the reaction and could be easily separated and reused. In contrast, the neat complexes were completely destroyed during the first run while changing colour from light yellow to dark brown. (3) Both conversion and specific rate (turnover frequency, TOF) increase when electron-withdrawing substituents (like –Cl, –Br, and $-NO_2$) are substituted in the aromatic ring (Table 1). Thus, TOF for Mn(III)Salen, $Mn(III)Cl_2$Salen, $Mn(III)Br_2$Salen, and $Mn(III)(NO_2)_2$Salen are 28, 40, 45, and 41, respectively. A similar trend is also observed for the zeolite-encapsulated catalysts. (4) Conversion of styrene (per unit weight of the catalyst sample) decreases on encapsulation (e.g., 78.8 and 54.8 mol% for Mn(III)Salen and Mn(III)Salen–X, respectively). This is due to the diffusional resistance encountered by the

Table 7
Oxidation of styrene over Mn–Salens with O_2 (air)

Catalyst	Styrene conversion (mol%)	TOF (h^{-1})	Products (mol%)			
			BA	SO	PA	Others
Mn(III)Salen	78.8	28	52.0	32.5	8.1	7.4
Mn(III)Salen–X	54.8	761	66.7	27.7	–	5.6
$Mn(III)Cl_2$Salen	93.1	40	75.0	13.4	5.3	6.3
$Mn(III)Cl_2$Salen–X	73.3	1292	75.7	18.4	–	5.9
$Mn(III)Br_2$Salen	87.0	45	58.4	24.7	8.4	8.5
$Mn(III)Br_2$Salen–X	68.7	852	75.8	18.6	–	5.6
$Mn(III)(NO_2)_2$Salen	91	41	58.1	27.8	4.7	9.4
$Mn(III)(NO_2)_2$Salen–X	75.4	1439	65.5	25.9	2.1	6.5

Reaction conditions: 343 K; styrene = 5 g; solvent, CH_3CN = 5 g; air feed = 4.9 l/h; catalyst wt. = 0.05 g; TBHP = 0.1 g; reaction time = 10 h (neat complexes) and 12 h (encapsulated catalysts); BA = benzaldehyde; SO = styrene oxide; PA = phenylacetaldehyde; Others = benzene 1,2-ethanediol, benzoic acid and other unidentified high boilers.
TOF = turnover frequency, moles of styrene converted per mole of manganese per h.

substrate styrene molecules in reaching the active sites located inside the supercages of zeolite crystals. (5) TOF values (per unit weight of the manganese salens), however, are enhanced by an order of magnitude on encapsulation. This is probably due to the isolation of the Mn sites in the zeolite cavities. (6) The salen ligand alone in the absence of the Mn metal was not catalytically active. (7) Even though styrene could be oxidised over the above catalysts using air alone, the conversion levels were low (under the conditions of Table 7), and the products were polymeric in nature. There is, hence, a synergistic enhancement in TOF when both O_2 and TBHP were used as the oxidants. The synergistic role of TBHP (along with O_2) in enhancing the rate of oxidation reactions has been reported recently [19,20], though the mechanism is not very clear. (8) The formation of phenyl acetaldehyde (PA) is suppressed on encapsulating the complexes inside the cavities of the zeolites (Table 7). In fact, except in the case of Mn(III)$(NO_2)_2$Salen–X, PA is not observed at all among the products from other encapsulated complexes.

One of the major drawbacks of homogeneous metal complexes as catalysts is their irreversible deactivation due to formation of μ-oxo and μ-peroxo dimeric and other polymeric species especially when using dioxygen as the oxidant. Since the formation of these bulky dimeric/polymeric species is sterically impossible when the monomeric complex is encapsulated and physically confined within the supercages of zeolite X, it was anticipated that encapsulated catalysts would be more rugged and can be recycled for use. The data in Table 8 support the above hypothesis. As mentioned earlier, the neat complexes could not be recycled even once as they lost their catalytic activity after use. By contrast, the encapsulated, solid catalysts could be filtered, washed with a solvent (to remove polymeric species formed from styrene) and reused without major loss in activity. Any loss in activity, (as seen, for example, in Table 8 when using CH_3CN as solvent) is reversible and due more to polymeric material deposited in the pores of the zeolite, than to the destruction of the active metal complex. Hence, when acetone, a better solvent for the polymeric matter, is used as the solvent, the pores are continuously cleansed with only a marginal loss in catalytic activity on reuse. Comparing our present results with the earlier data on the epoxidation of styrene over a titanium silicate molecular sieve using H_2O_2 as the oxidant [16], we observe that the selectivity for styrene oxide is higher, and that for phenyl acetaldehyde, correspondingly lower over encapsulated Mn salens. The lower acidity of the present catalysts probably suppresses the further isomerisation of styrene oxide to phenylacetaldehyde. The benzaldehyde levels are, however, relatively higher, suggesting a greater contribution of the radical route in the MnSalen–O_2 system compared to the titanosilicate–H_2O_2 system.

Table 8
Oxidation of styrene over Mn(III)Br_2Salen–X: influence of catalyst recycle

Cycle	Solvent	Styrene conversion (mol%)	Products (mol%)		
			BA	SO	Others
I	CH_3CN	68.7	72.9	18.5	8.4
II	CH_3CN	64.9	77	18.2	5.2
III	CH_3CN	60.7	75.1	20.0	4.9
I	Acetone	69.9	72.8	18.9	8.3
II	Acetone	68.9	74.3	19.1	6.6

See Table 7 for other details.

4. Summary and conclusions

Salen and substituted salen complexes of manganese(III) have been encapsulated in the supercages of zeolite X by synthesizing the faujasite zeolite around the metal complex molecules dissolved in the zeolite synthesis medium. The resulting catalysts have been characterized by various spectroscopic (IR, UV–Vis and EPR), thermal analysis and adsorption techniques. Both the electron withdrawing character

and geometric size of the substituents on the aromatic rings of the salen ligands influence the extent of encapsulation, as well as the relative stability of the various oxidation states of Mn. While bulky substituents like Br enhance the amount of metal complex encapsulated, electron-withdrawing groups like $-NO_2$ seem to lower the extent of encapsulation. The chemical stoichiometry and the structural integrity of the complex is preserved in the encapsulated state. Cyclic voltammetric measurements, however, indicate significant differences in the electrochemical behaviour of Mn ions (the active site in oxidation reactions) in the encapsulated state from that of the neat complexes. The zeolite matrix facilitates the reduction of Mn(III) to Mn(II), suggesting that it behaves like an electron-withdrawing substituent.

In the aerobic oxidation of styrene over these complexes, the catalytic efficiency (turnover frequency) of zeolite-encapsulated complexes is much higher than that of the neat complexes. Electron-withdrawing substituents (like –Cl, –Br and $-NO_2$) on the aromatic ring enhance the rate of oxidation. The major oxidation products of styrene over the neat complexes are styrene epoxide, benzaldehyde and phenylacetaldehyde. One of the advantages of encapsulation is the absence of major irreversible catalyst deactivation. The neat complex in homogeneous solution was completely and irreversibly deactivated on use in the aerobic oxidation of styrene. On encapsulation, there was only a slight reversible loss in catalytic activity due to deposition of organic polymeric material. The catalyst could be recycled after removal of these organic polymer material by a suitable solvent such as acetone. The greater stability is attributed to the suppression of dimeric and other polymeric oxo complexes of Mn due to geometric constraints on their formation on encapsulation in zeolites.

Acknowledgements

SPV thanks the Department of Science and Technology, New Delhi for the award of Young Scientist Fellowship. We thank Dr. K. Vijayamohan, Physical Chemistry, for discussion, and members of the Catalysis Division for help and support.

References

[1] R.F. Parton, I.F.J. Vankelecom, M.J.A. Casselman, C.P. Bezoukhanova, J.B. Uytterhoeven, P.A. Jacob, Nature 370 (1994) 541.
[2] N. Herron, J. Coord. Chem. 19 (1986) 25.
[3] N. Herron, Inorg. Chem. 25 (1988) 4714.
[4] D.E. De Vos, F. Thibault-Starzyk, P.A. Jacobs, Angew. Chem. Int. Ed. Engl. 33 (1994) 431.
[5] N. Herron, Chem. Tech. 9 (1989) 542.
[6] S. Kowalak, R.C. Weiss, K.J. Balkus Jr., J. Chem. Soc. Chem. Commun. (1991) 57.
[7] C. Bowers, P.K. Dutta, J. Catal. 122 (1990) 271.
[8] K.J. Balkus Jr., C.D. Hargis, S. Kowalak, ACS Symp. Ser. 499 (1992) 347.
[9] P.P. Kuops-Gerrits, D.E. De Vos, P.A. Jacobs, J. Mol. Catal.: A Chem. 117 (1997) 57.
[10] D.B. Ogunurumi, T. Bein, Chem. Commun. (1997) 901.
[11] R. Irie, N. Hosoya, T. Katasuki, Synlett. (1994) 255.
[12] T. Katasuki, Coord. Chem. Rev. 140 (1995) 189, and the references therein.
[13] W. Zhang, J.L. Loebach, S.R. Wilson, E.N. Jacobsen, J. Am. Chem. Soc. 112 (1990) 2801.
[14] K.J. Balkus Jr., A.G. Gabrielov, J. Inclusion Phen. Mol. Recognition Chem. 21 (1995) 173.
[15] H. Diegruber, P.J. Plath, G. Schultz-Ekloff, J. Mol. Catal. 24 (1984) 115.
[16] W.M. Coleman, R.K. Boggess, J.W. Hughes, L.T. Taylor, Inorg. Chem. 20 (1981) 700.
[17] F. Bedioui, L. Roue, E. Briot, J. Devynck, S.L. Bell, K.J. Balkus Jr., J. Electroanal. Chem. 19 (1994) 337.
[18] C. Romans, Y. Oliver Su, K.S. Michael, A.M. Kathleen, K. Dongho, T.G. John, G.S. Thomas, J. Am. Chem. Soc. 110 (1988) 4158.
[19] T.G. John, K.S. Michael, J. Am. Chem. Soc. 110 (1988) 8628.
[20] A.M. Bond, F. Scholz, Langmuir 7 (1991) 3197.
[21] A.J. Bard, L.R. Faulkner, in: Electrochemical Methods, Wiley, New York, 1980.